Investigations of orientational order for an antiferroelectric liquid crystal by polarized Raman scattering measurements

Naoki Hayashi and Tatsuhisa Kato
Institute for Molecular Science, Myodaiji, Okazaki 444-8585, Japan
(Received 10 April 2000; published 24 January 2001)

The orientational ordering of the antiferroelectric liquid crystal molecules, 4-(1-methylheptyloxycarbonyl)phenyl 4′-octyloxybiphenyl-4-carboxylate was investigated in the series of the successive smectic phases by means of polarized Raman scattering measurement without any external field. An improved equation for the analysis of the polarized Raman intensity was derived as a function of an incident laser polarization and the orientational order parameters. Even in the chiral smectic phases, some apparent orientational order parameters could be defined by the proper corrections for the smectic layer structure and an optical disturbance. An unusual change of the orientational order parameters was observed with decrease in temperature. It was concluded that the irregular variation of the order parameter stemmed from the biaxiality of the molecular orientational distribution, which was attributed to the hindrance of molecular rotation around its long axis.

DOI: 10.1103/PhysRevE.63.021706 PACS number(s): 61.30.−v

I. INTRODUCTION

Since Chandani *et al.* had discovered an antiferroelectric liquid crystal phase in MHPOBC [4-(1-methylheptyloxycarbonyl)phenyl 4′-octyloxybiphenyl-4-carboxylate] [1,2], the mechanisms of the successive phase transitions and the appearances of the subphases have been investigated by various methods with interests in science as well as in applications. The phase sequence and the transition temperatures of the optically pure MHPOBC are as below: isotropic −148 °C−smectic-A (SmA)−122 °C−smectic-C^*_α (SmC^*_α)−120.9 °C−smectic-C^* (SmC^*)−119.2 °C−smectic-C^*_γ (SmC^*_γ)−118.4 °C−smectic-C^*_A (SmC^*_A)−65 °C−crystal [3,4].

It was found that the molecules tilt opposite each other in the adjacent layers of SmC^*_A phase that shows an antiferroelectricity [5–8], and tilt opposite once with every three layers of SmC^*_γ phase, which shows a ferrielectricity [7–10]. A devil's staircase structure was proposed for SmC^*_α, which was based on the Ising model [11,12]. This phase does not show a single fixed structure but consists of the layered texture of ferroelectric and antiferroelectric layers, which pile up with the temperature dependent ratio [13,14]. SmC^* and the subphases exhibit helicoidal structure as a whole. Some experiments showed the peculiar structures of MHPOBC that play important roles for the appearance of the subphases and phase transitions, i.e., the vent structure [15,16] and molecular interactions or recognition in adjacent layers [17]. Moreover, it was observed under an electric field by infrared (IR) absorbance measurements that the rotation of the C═O group around the molecular long axis was hindered and the biased directions were different in SmC^* and SmC_A phase [18,19].

If the liquid crystal molecule is assumed as a rigid cylindrical rod in the uniaxial nematic or SmA phases, the molecular orientational distribution function $f(\beta)$ can be expanded in terms of Legendre polynomials $P_L(\cos\beta)$ [20,21],

$$f(\beta)=\sum_{L=\text{even}}\frac{2L+1}{8\pi^2}\langle P_L(\cos\beta)\rangle P_L(\cos\beta), \qquad (1)$$

where β is the angle between the individual molecular long axis and the center of orientational ordering. $\langle P_L(\cos\beta)\rangle$ is the orientational order parameter and is defined as below

$$\langle P_L(\cos\beta)\rangle=\int_0^\pi \sin\beta\, d\beta\, P_L(\cos\beta) f(\beta), \qquad (2)$$

here we denote a thermal average by $\langle\cdots\rangle$. The orientational order parameters can be evaluated by some spectroscopic methods [22]; i.e., polarized vibrational Raman scattering measurements [20,23–27], electron paramagnetic resonance (EPR) [28], NMR [29,30], IR [18,31,32], and so on. Especially the polarized vibrational Raman scattering measurements can give the estimation of not only the second order parameter $\langle P_2(\cos\beta)\rangle$ but also the fourth one $\langle P_4(\cos\beta)\rangle$.

Experimentally, some optical phenomena disturb the data analysis of the Raman scattering measurement, for example, the effects of the birefringence of the ordered liquid crystal. In order to avoid the disturbance by the birefringence, the parallel and perpendicular configuration with the optic axis of the liquid crystal is generally adopted for the polarized Raman scattering measurements. There are plenty of reports on the measurement of the order parameters in the nematic and SmA phases so far [20,23–27]. The order parameters of MHPOBC have been already reported in SmA phase [24]. On the other hand the analysis of the phases other than the uniaxial nematic and SmA phases becomes more complicated. In phases other than uniaxial ones, the Raman scattering intensities depend on the way smectic layers are piled up. Under the proper correction of the optical disturbance originated from the smectic layer structure, however, the orientational order parameters $\langle P_2(\cos\beta)\rangle$ and $\langle P_4(\cos\beta)\rangle$ can be defined as long as liquid crystal molecules uniaxially distribute within a layer. In this paper the correction for the analysis in SmC^* and the subphases of MHPOBC will be derived,

 ©2001 The American Physical Society

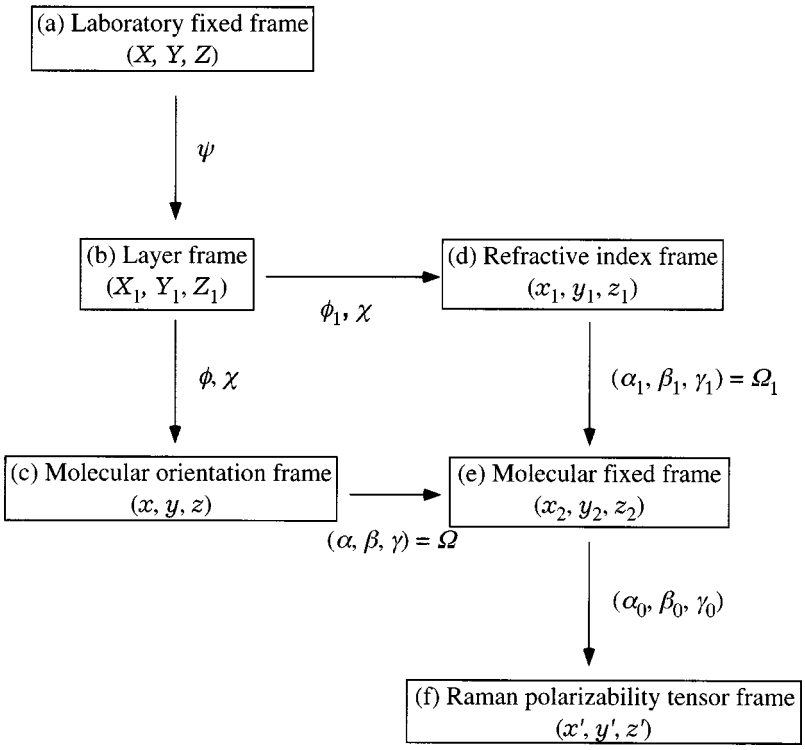

FIG. 1. Schematic diagram of coordinate system. The details are described in theoretical treatment section.

which take account of the peculiar optical disturbance by the following origins, i.e., the tilt angle of the molecular axis with the smectic layer normal, the spiral structure, and the layer tilt angle due to the chevron layer structures [17,33–37].

II. THEORETICAL TREATMENTS

The molecular orientational order parameter is obtained by the evaluation of the polarized Raman scattering intensity [20,21]. The backscattering configuration for the homogeneously aligned sandwich cell of the smectic phase liquid crystals is assumed here. It is necessary to define the orientational relation between the individual molecules and a reference coordinate system for the description of the molecular orientational distribution. Raman polarizability tensors of the individual molecules were described in the reference coordinate system by using several Cartesian coordinate systems that are based on the smectic layer structure, and the transformation among the coordinate system is explained here. A schematic diagram and the drawing of the coordinate system are given in Figs. 1 and 2, respectively. The coordinate systems are defined according to Figs. 1(a)–1(f). (a) A laboratory fixed frame is the reference coordinate system that is defined by X, Y, and Z with respect to the sample cell [Fig. 2(a)], the YZ plane is parallel to the glass substrate of the cell. The incident laser beam comes into the cell and the scattered light goes back along the X axis. (b) A layer frame is defined by X_1, Y_1, and Z_1 on the layer of smectic phase [Fig. 2(b)]. The Z_1 axis is parallel to the layer normal and tilts from the Z axis by the angle $+\psi$ or $-\psi$ because the layer is inclined from the glass plates by the chevron layer structure. The Y_1 axis is parallel to the Y axis. (c) A molecular orientation frame is defined by x, y, and z for one smectic layer [Fig. 2(c)]. The z axis is the center of the molecular orientational distribution in this layer. The rotational transformation from the layer frame to the molecular orientation frame is described by the angles of χ and ϕ. χ is the angle between the c director and the X_1 axis. ϕ is the angle between the z axis and the layer normal. In SmA phase, ϕ

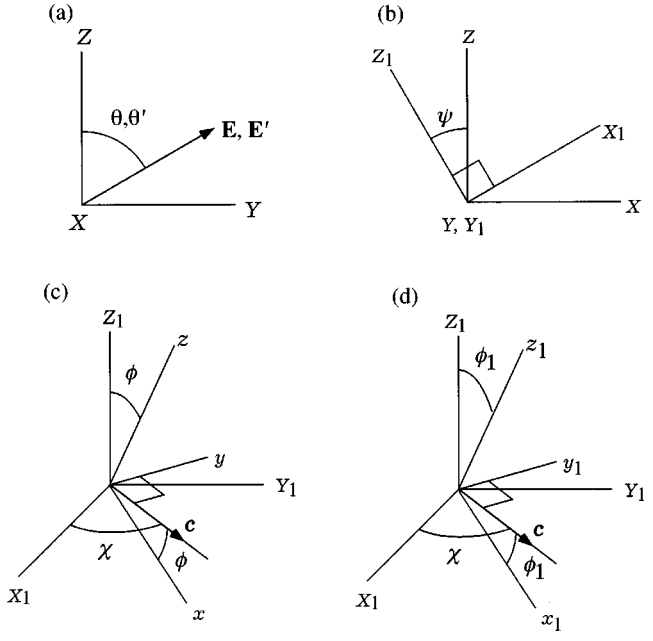

FIG. 2. The defined coordinate systems. (a) The laboratory fixed frame and the electric fields of incident and scattering lights. (b) The laboratory fixed frame and the layer fixed frame. (c) The layer frame and the molecular orientation frame. (d) The layer frame and the refractive index frame.

$=0$ and the molecular orientation frame coincides with the layer frame. (d) A refractive index frame is defined by x_1, y_1, and z_1 [Fig. 2(d)]. These axes are identical with optic elasticity axes and refractive indices are defined in this frame. The refractive index frame is not the same as the molecular orientation frame in the phase with helical structure, if the helical pitch is larger than a wavelength of light, because the optical property is given by an average over helically twisted layers with the wavelength of light. However, at the center of these layers, the averaged optical plane, defined as a plane containing two optic axes, is parallel to the xz plane of the molecular orientation frame in SmC^*, SmC^*_γ, and SmC^*_A phase of MHPOBC system [9]. Therefore, the transformation from layer frame to the refractive index frame is defined by χ and ϕ_1 as the analog of molecular orientation frame. (e) A molecular fixed frame is defined by x_2, y_2, and z_2 on the individual molecules. The z_2 axis is defined to be parallel to the molecular long axis. α, β, and γ are defined as the Euler angles that transform the molecular orientation frame to the molecular fixed frame. (f) A Raman tensor frame is defined by x', y', and z'. In this frame the Raman tensor of a vibrational mode for a particular molecule is diagonalized and has the form of

$$\begin{pmatrix} \alpha_{x'x'} & & \\ & \alpha_{y'y'} & \\ & & \alpha_{z'z'} \end{pmatrix}.$$

α_{ll} ($l=x',y',z'$) is a ll component of the Raman tensor in this frame and $\alpha_{z'z'}$ is the largest. The Euler angles $(\alpha_0,\beta_0,\gamma_0)$ transform the molecular fixed frame to this frame.

Now it is assumed that the polarization vectors of the incident light and the scattering light are within the YZ plane and make the angles θ and θ' with Z axis, respectively [Fig. 2(a)]. $\mathbf{E}_{(X)}$ and $\mathbf{E}'_{(X)}$ are defined as the electric fields of incident light and scattering light at a depth X from the surface of the liquid crystal, and they can be decomposed into x_1, y_1, and z_1 components of the refractive index frame,

$$\mathbf{E}_{(X)}=E_{x_1}e^{-i\delta x_1}\hat{x}_1+E_{y_1}e^{-i\delta y_1}\hat{y}_1+E_{z_1}\hat{z}_1, \tag{3}$$

$$\mathbf{E}'_{(X)}=E'_{x_1}e^{-i\delta' x_1}\hat{x}_1+E'_{y_1}e^{-i\delta' y_1}\hat{y}_1+E'_{z_1}\hat{z}_1, \tag{4}$$

where the phase factors of $e^{-i\delta x_1}$, $e^{-i\delta y_1}$, $e^{-i\delta' x_1}$, and $e^{-i\delta' y_1}$ are introduced to give the correction for the retardation effect that is due to the birefringence of the ordered liquid crystal. δx_1, δy_1, $\delta' x_1$, and $\delta' y_1$ are the phase difference of x_1 and y_1 components with z_1.

The peculiar structure of each smectic phase should be reflected on the further effective optical correction for the electric fields of the incident laser light and the scattering light. The effective corrections for each smectic phase are summarized in Appendix A. For example, SmC^* and the other subphases exhibit helical structure and optical biaxiality; then one should give a close examination for the proper correction. The relation between the molecular orientation frame and the refractive index frame is also described in Appendix A.

When the measured area is sufficiently large compared with the helical pitch, the Raman intensity is obtained by averaging for one period of the helical pitch,

$$I(\theta,\theta')\propto\int_0^{\pi}\sin\phi\,d\phi\int_0^{2\pi}d\chi\int_0^{d}dX\langle|\alpha_{\theta\theta',(X)}|^2\rangle, \tag{5}$$

where $\alpha_{\theta\theta',(X)}$ is the Raman polarizability tensor described in the molecular orientation frame, d is a sample thickness, and $\langle|\alpha_{\theta\theta',(X)}|^2\rangle$ is an integrated value over the orientation of the liquid crystal,

$$\langle|\alpha_{\theta\theta',(X)}|^2\rangle=\int d\Omega|\alpha_{\theta\theta',(X)}|^2 f(\Omega). \tag{6}$$

$f(\Omega)$ is the orientational distribution function of the molecular long axis or z_2 axis with respect to the z axis and Ω denotes Euler angles (α,β,γ). Furthermore, the effect of a refracting angle on the Raman scattering intensity must be taken into consideration and the measured intensity is obtained from

$$I_{\mathrm{mes}}(\theta,\theta')=\frac{I(\theta,\theta')}{n(\theta')^2}, \tag{7}$$

where $n(\theta')$ is the refractive index at θ' given by

$$n(\theta')=\frac{n_Z n_Y}{\sqrt{n_Z^2\sin^2\theta'+n_Y^2\cos^2\theta'}}. \tag{8}$$

n_Y and n_Z are refractive indices of a liquid crystal material for the light polarized along the Y axis and the Z axis, respectively. The combination of θ and θ' will be fixed at two configurations of $\theta'=\theta$ and $\theta'=\theta+\pi/2$. Here it was assumed that the ideal helical structure was formed in the chiral smectic phases, that is, the molecular orientational distribution was uniaxial with respect to the layer frame. With the aid of the computer software MATHEMATICA 2.2 (Wolfram Research, Inc.), Eqs. (5) and (7) are evaluated and rearranged. When the sample thickness is sufficiently large compared to the wavelengths of the incident and the scattering lights, the polarized Raman intensities are represented as a function of θ and the orientational order parameters;

$$\begin{aligned} I(\theta,\theta)_{\mathrm{mes}}&\equiv I_{\parallel}(\theta)\\ &=C_1(\cos\theta)+C_2(\cos\theta)\langle P_2(\cos\beta_{\mathrm{app}})\rangle\\ &\quad+C_3(\cos\theta)\langle P_4(\cos\beta_{\mathrm{app}})\rangle+C_4(\cos\theta)R, \end{aligned} \tag{9}$$

$$\begin{aligned} I(\theta,\theta+\pi/2)_{\mathrm{mes}}&\equiv I_{\perp}(\theta)\\ &=C_5(\cos\theta)+C_6(\cos\theta)\langle P_2(\cos\beta_{\mathrm{app}})\rangle\\ &\quad+C_7(\cos\theta)\langle P_4(\cos\beta_{\mathrm{app}})\rangle-C_4(\cos\theta)R. \end{aligned} \tag{10}$$

$C_1(\cos\theta)$ to $C_7(\cos\theta)$ are the fourth order functions of $\cos\theta$, whose coefficients depend on ϕ and ψ, the refractive index of the liquid crystal material and the glass substrate, helical pitch, and the Raman tensor. The coefficients for odd order terms of $C_1(\cos\theta)$ to $C_7(\cos\theta)$ are zero because of the symmetry of the system. R represents the component of retardation amplitude that depends on the sample thickness. $\langle P_2(\cos\beta_{\rm app})\rangle$ and $\langle P_4(\cos\beta_{\rm app})\rangle$ are the second and the fourth orientational order parameters of the z' axis of Raman tensor with respect to the Z_1 axis, and $\beta_{\rm app}$ is the angle between the z' axis and the Z_1 axis. It should be noticed that the effect of the retardation on the Raman intensity is not zero even if $\theta=0°$ or $\theta=90°$ when the refractive index frame is inclined with respect to the incident light and the scattering light (e.g., smectic phase with helical structure and/or $\psi\neq 0$.) Therefore, the orientational order parameters cannot be evaluated properly by the measurements of depolarization ratios only at $\theta=0°$ and $\theta=90°$, and at least three different measurement points of θ are needed.

It is supposed that the Raman tensor is uniaxial, namely, $\alpha_{x'x'}=\alpha_{y'y'}=\alpha_\perp$ and $\alpha_{z'z'}=\alpha_\parallel$ and the z' axis of the Raman tensor can rotate freely around the z_2 axis of the molecular fixed frame. Then the orientational molecular distribution defined in one layer has a cylindrical symmetry and $\langle P_2(\cos\beta_{\rm app})\rangle$ and $\langle P_4(\cos\beta_{\rm app})\rangle$ could be rewritten with the molecular orientational order parameters $\langle P_2(\cos\beta)\rangle$ and $\langle P_4(\cos\beta)\rangle$ with respect to z axis in the molecular orientation frame as following equations:

$$\begin{aligned}\langle P_2(\cos\beta_{\rm app})\rangle &= \tfrac{1}{2}(3\cos^2\phi-1)\tfrac{1}{2}(3\cos^2\beta_0-1)\\ &\quad\times\langle P_2(\cos\beta)\rangle\\ &= \tfrac{1}{2}(3\cos^2\phi-1)\langle P_2(\cos\beta')\rangle. \qquad (11)\end{aligned}$$

$$\begin{aligned}\langle P_4(\cos\beta_{\rm app})\rangle &= \tfrac{1}{8}(35\cos^4\phi-30\cos^2\phi+3)\\ &\quad\times\tfrac{1}{8}(35\cos^4\beta_0-30\cos^2\beta_0+3)\\ &\quad\times\langle P_4(\cos\beta)\rangle\\ &= \tfrac{1}{8}(35\cos^4\phi-30\cos^2\phi+3)\langle P_4(\cos\beta')\rangle, \qquad (12)\end{aligned}$$

where β_0 is the angle between z' axis and z_2 axis, $\langle P_2(\cos\beta')\rangle$ and $\langle P_4(\cos\beta')\rangle$ are the orientational order parameters of the z' axis of the Raman tensor with respect to z axis. It should be noticed that apparent values of $\langle P_2(\cos\beta_{\rm app})\rangle$ and $\langle P_4(\cos\beta_{\rm app})\rangle$ would be reduced by ϕ and β_0, and even become zero with the specific value of ϕ and β_0 at the so-called magic angle value.

In isotropic phase, both $\langle P_2(\cos\beta)\rangle$ and $\langle P_4(\cos\beta)\rangle$ are zero and the depolarization ratio $R_{\rm iso}$ is calculated as

$$R_{\rm iso}\equiv I_\perp/I_\parallel = 3b^2/(45a^2+4b^2), \qquad (13)$$

where a and b correspond to the average value and the anisotropy of the Raman tensor, respectively, and calculated by

$$a=\tfrac{1}{3}(\alpha_\parallel+2\alpha_\perp), \qquad (14)$$

$$b=(\alpha_\parallel-\alpha_\perp). \qquad (15)$$

Thus the orientational order parameter is obtained from the analysis of $I_\parallel(\theta)$, $I_\perp(\theta)$, and $R_{\rm iso}$ using Eqs. (9)–(13) if the structural parameters are known. It should be noticed that only $\langle P_2(\cos\beta')\rangle$,$\langle P_4(\cos\beta')\rangle$ are possible to be evaluated from these equations because β_0 is an unknown parameter, here.

III. EXPERIMENTS

The molecular structure of (S)-MHPOBC is shown here

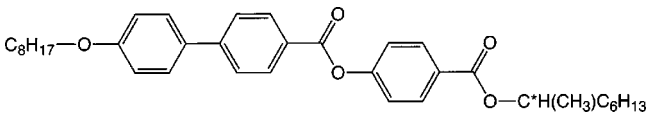

which has three benzene rings and two ester bonds, one is in a center of the core part and another is attached to the end of the core part or the chiral part. In order to confirm the purity of the sample, the phase transition temperatures were measured by the differential scanning calorimeter of TA Instruments DSC 2920 [2,3]. The experimental cell was prepared as follows and the homogeneous alignment was accomplished. The sample was sandwiched between two ITO-coated quartz plates with the thickness of 25 μm by using poly(ethylene terephthalate) spacers. The quartz plates were spin coated with polyimide and one of them was rubbed in one direction. The cell was set on the rotating stage, which was equipped with the heat controller that adjusted temperature with the accuracy of ± 0.1 °C with a controller (Yokogawa, UP550). The condition of alignment was checked by a polarizing optical microscope. Many focal conics were observed except for SmA phase, but the whole image was sufficiently dark and it was assumed that they did not affect Raman intensities much. Hence, the disturbance of alignment by these defects was ignored [24].

The polarized Raman spectra were measured by the following system. The green light at 514.5 nm from an argon ion laser (Spectra-Physics, BeamLok 2060) was used for excitation. The exciting light was polarized by a glan laser prism. Scattered light was collected by a lens in the back light scattering configuration and introduced to a polarizer, a Raman notch filter, and a monochromator (Spex, 270M) combined with a multichannel detector (Princeton Instruments, IPDA 512). The incident laser power was set at 0.5 W and the slit width of the monochromator was 50 μm in all measurements. The depolarization ratios of Raman lines were estimated by the measurement for isotropic phase at 150 °C. The Raman lines were deconvoluted with Lorentzian function to obtain integrated intensities.

Polarized Raman spectra were measured at various orientations of the incident laser polarization, and the angle of the orientation between the laser polarization and liquid crystal alignment were set from 0° to 180° at steps of 10°. The temperature was varied from 90 to 140 °C. In order to confirm the phase of the sample during the Raman scattering measurement, simultaneous monitoring of the capacitance of the cell was done by a LCR meter (YHP, 4262A), as shown

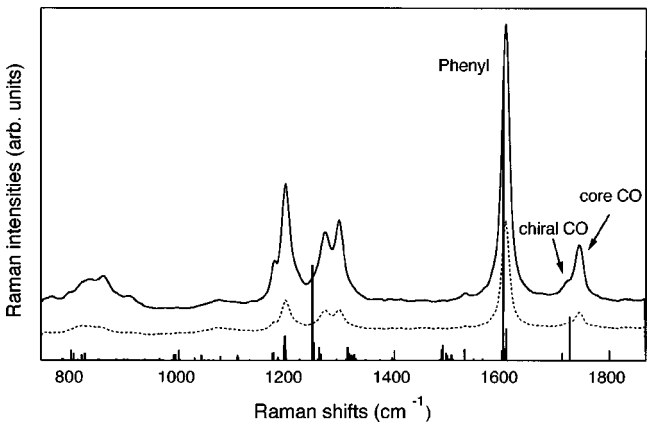

FIG. 3. The polarized Raman spectrum in isotropic phase at 150 °C (solid line for $I_{\parallel}$; broken line for $I_{\perp}$) and the Raman activities obtained from *ab initio* calculations (sticks).

in Fig. 4. The frequency of the test signal was 1 kHz. In the ferroelectric phase (SmC^*) the capacitance shows a peak value due to a spontaneous polarization, but in the antiferroelectric (SmC_A^*) and paraelectric phase (SmA), it drops down. In the ferrielectric phases (SmC_α^* and SmC_γ^*), it exhibits decreasing values [7,17,39].

The theoretical predictions of the Raman tensors were carried out by an *ab initio* restricted Hartree-Fock calculation with the 3-21G basis set using the GAUSSIAN 94 package [40].

The refractive indices of liquid crystal for which the light is polarized parallel and perpendicular to the Z_1 axis, $n_{\parallel}$ and $n_{\perp}$, were obtained from Ref. [9]. The refractive index of quartz plates n_g was 1.46.

Helical pitches were measured by the diffraction method [41,42] with He-Ne laser at 632.8 nm.

IV. RESULTS

Figure 3 shows the polarized Raman spectra in isotropic phase at 150 °C. Three Raman lines were investigated, i.e., C—C stretching mode of three benzene rings at 1600 cm^{-1}, which is abbreviated as ''phenyl,'' C═O stretching mode of chiral carbonyl group at 1720 cm^{-1}, ''chiral CO,'' and C═O stretching mode of core carbonyl group at 1740 cm^{-1}, ''core CO'' [24,43]. Their depolarization ratios are listed in Table I. The shifts of the Raman lines in crystal-SmI^* phase transition [43] have been reported, but any shift and change of line width were not observed in the successive phase transitions from isotropic to SmC_A^* phase. This shows that no major changes occur either in the normal coordinates or in the intermolecular interactions during these phase transitions.

The results of an *ab initio* calculation are listed in Table I. The calculated depolarization ratios of three Raman lines in question generally agree with the observed values in isotropic phase. The Raman activities predicted by the *ab initio* calculations are shown with solid lines in Fig. 3. Their Raman shifts and activities are consistent with measured spectra. The calculated Raman tensors are also listed in the table. It was confirmed that each $\alpha_{z'z'}$ is considerably large compared to other components and thus these Raman lines are

TABLE I. *Ab initio* calculation results. α_{ll} ($l=x',y',z'$) is a ll component of the Raman tensor in Cartesian coordinate of Raman tensor frame.

	Depolarization ratios		Raman tensors		
Raman lines	Obs.	Calc.	$\alpha_{x'x'}$	$\alpha_{y'y'}$	$\alpha_{z'z'}$
Phenyl	0.382	0.389	0.13	0.50	10.6
Chiral CO	0.221	0.298	0.01	0.10	1.75
Core CO	0.263	0.280	0.01	0.45	4.25

suitable for the evaluations of the orientational order parameters. The calculated angles between the z' axis and the biphenyl link are about 10° for phenyl line and chiral CO line, and almost 0° for core CO line. It was found that all of the z' axes of the Raman tensors lie towards the molecular long axis.

The capacitance and the polarized component of the phenyl line at $\theta=0$ were obtained by the parallel measurement in the cooling process. The results are plotted as a function of the temperature in Fig. 4. The capacitance gradually decreased from the high temperature side down to 120 °C, then it leaped to the maximum at 115 °C. Thereafter, it dropped around 113 °C and became steady. On the other hand, the Raman scattering intensity decreased from 118 °C to 113 °C. This decrease in the Raman intensity would be mainly owing to the increase of the ϕ after SmA-SmC_α^* phase transition [24], as explained before. [Refer to Eqs. (9)–(12).] The drastic change of the observed capacitance gave a good indication of the transition temperature, as shown in Fig. 4.

The helical pitches of the homogeneous cell used here were three or four times longer than the value reported for free standing film in SmC^* and SmC_A^* phase [5,44]; i.e., 1700 nm in the SmC^* phase and 2000–4000 nm in the SmC_A^* phase. The substrates affect the helical pitch by wall anchoring effects. In SmC_γ^* phase, the helical pitch was too long to be measured by the diffraction method. Judging from

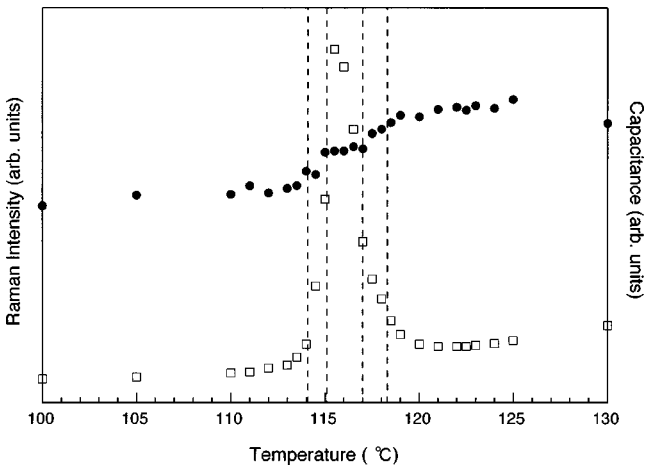

FIG. 4. Temperature dependence of the capacitance (□) and the polarized intensity of phenyl line (●). The vertical broken lines show transition temperatures. The phase sequence is SmA-SmC_α^*-SmC^*-SmC_γ^*-SmC_A^*.

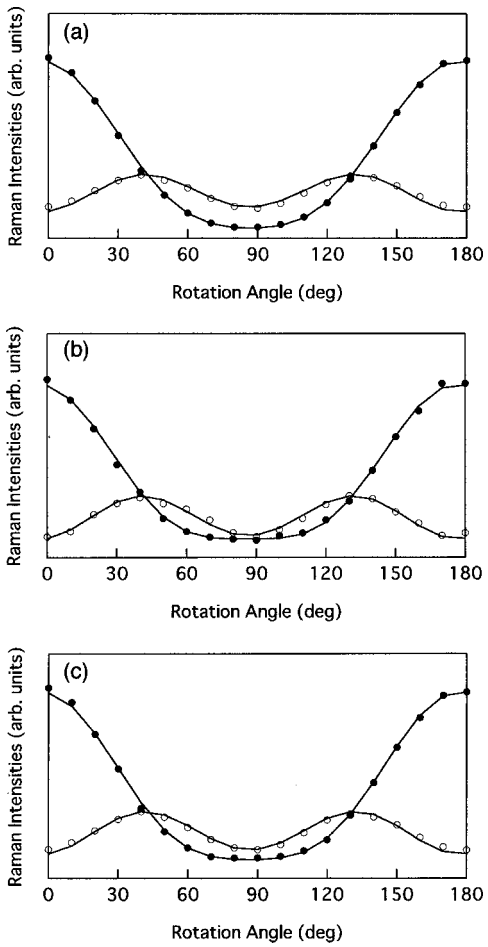

FIG. 5. The dependence of the polarized Raman intensities on the incident laser polarization at 115.6 °C (SmC^* phase) for phenyl line (a), core CO line (b), chiral CO line (c). Solid marks are $I_{\parallel}(\theta)$ and open marks are $I_{\perp}(\theta)$. The lines show the results of the fitting with Eqs. (9) and (10).

the values in SmC^* and SmC_A^* phase, it was estimated around 8000 nm.

The polarized and depolarized components of the Raman scattering for the three Raman lines measured at 115.6 °C (SmC^* phase) are plotted against the incident laser polarization in Fig. 5. The solid lines show the fitting results by the Eqs. (9)–(13), where the parameters *a*, *b*, $\langle P_2(\cos\beta')\rangle$, $\langle P_4(\cos\beta')\rangle$, and R were determined by the fitting procedure under the assumption of the cylindrical symmetric Raman polarizability tensors for a molecule. The other parameters used here are summarized in Table II, where layer tilt angles ψ and molecular tilt angles ϕ had been given by previous workers [17,24], and *H* is the helical pitch.

The obtained orientational order parameters $\langle P_2(\cos\beta')\rangle$ and $\langle P_4(\cos\beta')\rangle$ are shown in Fig. 6. Sticks show the errors that were evaluated from the standard deviation of the fitting process. The error for $\langle P_4(\cos\beta')\rangle$ is larger than $\langle P_2(\cos\beta')\rangle$ because of the larger sensitivity to the Raman scattering intensity. In Sm*A* phase, the order parameter evaluated from the phenyl line is agreed with the values reported by Kim *et al.* [24]. All $\langle P_2(\cos\beta')\rangle$ gradually increased with decreasing temperature, as one generally expected for the ordering process of liquid crystal. It should be noted that a bit smaller value of $\langle P_2(\cos\beta')\rangle$ for core CO line than for the other lines was obtained. This small difference in the value would give the angle β_0 between the z' axis of the Raman tensor and the molecular long axis, as described in discussion. On the other hand, $\langle P_4(\cos\beta')\rangle$ exhibited drastic variation as temperature was decreased, that is, it smoothly increased in Sm*A* phase, scattered in SmC_α^*, SmC^*, SmC_γ^* phases, and dropped in SmC_A^* phase.

TABLE II. Parameters used in the fitting. n_Z, n_Y, ψ, and ϕ are taken from Refs. [9,17,24].

Phase	Temp. (°C)	n_Z[a]	n_Y[a]	ψ[b] (deg.)	ϕ[c] (deg.)	*H* (nm)
Sm*A*	140	1.63	1.50	6		
	130	1.63	1.50	7		
	121	1.63	1.50	8		
	118.4	1.63	1.50	10.5		
SmC_α^*	117.2	1.63	1.50	12	12	
SmC^*	115.6	1.63	1.50	13.5	15	1700
SmC_γ^*	114.8	1.63	1.50	14	16.5	8000
SmC_A^*	113	1.62	1.50	15	18.5	
	100	1.62	1.50	16.5	23	
	90	1.62	1.50	17	24.5	

[a]Reference [9].
[b]Reference [17].
[c]Reference [24].

V. DISCUSSION

A. Orientational order parameter in Sm*A* phase

In Sm*A* phase, $\langle P_2(\cos\beta')\rangle$ and $\langle P_4(\cos\beta')\rangle$ gradually increased with decreasing temperature. This phenomenon is as one generally would expect, for the ordering process of

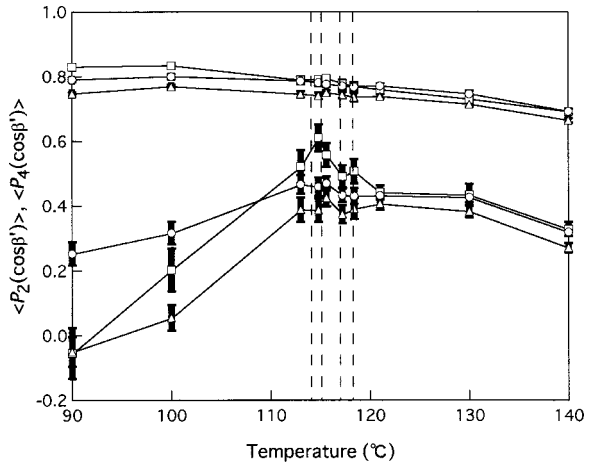

FIG. 6. The second and the fourth orientational order parameters, $\langle P_2(\cos\beta')\rangle$ and $P_4(\cos\beta')$; ○, phenyl line; △, core CO line; □, chiral CO line. The solid lines show $\langle P_2(\cos\beta')\rangle$ and the dotted lines show $P_4(\cos\beta')$. The vertical broken lines show transition temperatures.

liquid crystals. The small differences of $\langle P_2(\cos\beta')\rangle$ and $\langle P_4(\cos\beta')\rangle$ for core CO line from those for the other lines are noted in Fig. 6. According to Eqs. (11) and (12) the angle β_0 of core CO line is evaluated as 9° when z' axes of phenyl and chiral CO lines were assumed to be identical with the molecular long axis. The common statistics under the assumption of the cylindrical symmetry could be adopted for the molecular orientational distribution in Sm*A* phase.

B. The biaxial orientational distribution of molecules in Sm*C** and its subphase

The value of $\langle P_4(\cos\beta')\rangle$ exhibited a peculiar variation after SmC^*_α phase. The dispersion in variation in SmC^*_α, Sm*C**, SmC^*_γ phases and decrease in SmC^*_A phase are unusual under the assumption of the cylindrically symmetric orientational distribution of molecules. This discrepancy would be caused by the breakdown of the assumption of the uniaxiality for the molecular orientational distribution. It has been suggested that the rotation of the C═O group around the molecular long axis is hindered in Sm*C** and its subphases [18,19].

Now the orientational order parameters $\langle D^{(L)*}_{m'm}(\Omega)\rangle$ must be introduced to express the biaxiality of the molecular orientational distribution [20], and the polarized Raman intensities are given by the functions of $\langle D^{(L)*}_{m'm}(\Omega)\rangle$ and the structural parameters (see Appendix. B).

At present, it is supposed that molecular distribution is biaxial and the molecule can rotate around its long axis freely. Then,

$$\langle P_L(\cos\beta_{\rm app})\rangle = P_L(\cos\phi)P_L(\cos\beta_0)\sum_{m=-L}^{L}\langle D^{(L)*}_{0m}(\alpha,\beta)\rangle. \tag{16}$$

$\langle P_4(\cos\beta_{\rm app})\rangle$ is independent of γ, because the z' axis distributes uniaxially around z_2 axis. $\langle D^{(L)*}_{00}(\Omega)\rangle$ correspond to $\langle P_L(\cos\beta)\rangle$ and depends on only β. It was deduced from the above equation that the decrease of $\langle P_4(\cos\beta_{\rm app})\rangle$ in SmC^*_A phase was due to the terms $\langle D^{(L)*}_{0m}(\alpha,\beta)\rangle_{m\neq 0}$ and the different β_0 for each Raman line caused the scattering of $\langle P_4(\cos\beta_{\rm app})\rangle$ at lower temperature range than the Sm*A*-SmC^*_α phase transition. On the other hand, $\langle P_4(\cos\beta_{\rm app})\rangle$ of phenyl line and chiral CO line exchanged their order with each other in this phase. This phenomenon cannot be explained by Eq. (16), since β_0 is constant for the temperature variation and ϕ and $\langle D^{(L)*}_{0m}(\alpha,\beta)\rangle$ are independent of Raman line.

Accordingly, it was inferred that the molecular rotation around its long axis is hindered. Then Eq. (B3) is obtained. [See Appendix B and compare with Eqs. (11), (12), and (16).] It is supposed tentatively that the molecular rotation around its long axis is perfectly restricted as $\alpha=0$ and $\gamma=0$ and the Raman tensor of a molecule has a cylindrical symmetry. When $\alpha_0=0$, then $\beta_{\rm app}=\phi+\beta+\beta_0$ is obtained and $\langle P_L(\cos\beta_{\rm app})\rangle$ is reduced. Meanwhile when $\alpha_0=\pi$, $\beta_{\rm app}=\phi+\beta-\beta_0$ and $\langle P_L(\cos\beta_{\rm app})\rangle$ is increased. Similarly, when $\alpha=0$, $\gamma=\pi$, and $\alpha_0=0$, then $\beta_{\rm app}=\phi+\beta-\beta_0$. That is, $\langle P_L(\cos\beta_{\rm app})\rangle$ largely depends on the value of α_0, a hindered direction and a strength of hindrance to the molecular rotation around its long axis.

$\langle D^{(4)*}_{m'm}(\Omega)\rangle$ are higher order parameters than $\langle D^{(2)*}_{m'm}(\Omega)\rangle$. The higher order parameter generally exhibits sharper variation to the change of orientational distribution. On the other hand, $\langle D^{(4)*}_{00}(\Omega)\rangle$ is originally minor term than $\langle D^{(2)*}_{00}(\Omega)\rangle$. Then small disturbance by the $\langle D^{(4)*}_{m'm}(\Omega)\rangle$ looks much exaggerated to the minor term of $\langle D^{(4)*}_{00}(\Omega)\rangle$. This would be the reason why the apparent $\langle P_4(\cos\beta')\rangle$ showed more drastic reduction and scattering by the hindrance of molecular rotation than $\langle P_2(\cos\beta')\rangle$.

Following image could be drawn for a relation between the phase and the molecular orientational distribution. In Sm*A* phase, MHPOBC molecule distribute uniaxially around its director. After transition to SmC^*_α phase, the molecules tilt away from the helical axis, so that the orientational distribution could be biaxial. In this phase, the molecular rotation around its long axis might be somewhat hindered, and the apparent orientational order parameters show scattering due to different values of α_0 and β_0 for each Raman line. Then, in the SmC^*_A phase, the molecular rotation is rather hindered and the hindered direction might be changed as reported before [18,19] while the biaxiality of the molecular orientational distribution is increased, thus the apparent $\langle P_4(\cos\beta')\rangle$ is reduced.

VI. CONCLUSIONS

The equation of the polarized Raman intensity was derived as a function of the orientational order parameter and incident laser polarization, where it was taken into account how the structure influences the optical properties in Sm*C** and the subphases. The polarized Raman scattering measurements of MHPOBC without any external field were analyzed according to this equation, and the second and the fourth order orientational order parameters were evaluated in the successive smectic phases. The unusual decrease in the orientational order parameters were observed in SmC^*_A phases with decreasing temperature. It was indicated that they stemmed from the growth of the biaxiality of the molecular orientational distribution as temperature decreases because of the hindrance of the molecular rotation around its long axis.

ACKNOWLEDGMENT

We are grateful to Dr. Yukio Ouchi of Nagoya University for supplying MHPOBC material and preparing the sample cell.

APPENDIX A: THE STRUCTURES OF SMECTIC PHASES AND THE ELECTRIC FIELD OF THE INCIDENT AND THE SCATTERING LIGHT

1. Sm*A* phase

Sm*A* phase is optically uniaxial and $\phi=0$, so that the refractive index frame, the molecular orientation frame, and the layer frame are identical with each other. When a layer

tilt for the substrates ψ is taken into account [17,38], the electric fields of the incident and the scattering lights are given by

$$\mathbf{E}_{(X)}=e^{-i\delta x_1}(T_Z\sin\psi\cos\theta)\hat{x}_1+e^{-i\delta y_1}(T_Y\sin\theta)\hat{y}_1 +(T_Z\cos\psi\cos\theta)\hat{z}_1, \tag{A1}$$

$$\mathbf{E}'_{(X)}=e^{-i\delta' x_1}(T'_Z\sin\psi\cos\theta')\hat{x}_1+e^{-i\delta' y_1}(T'_Y\sin\theta')\hat{y}_1 +(T'_Z\cos\psi\cos\theta')\hat{z}_1. \tag{A2}$$

T_L and T'_L are transmission coefficients for L components of electric field at the interface between substrate and liquid crystal. They are calculated by

$$T_L=\frac{2n_g}{n_g+n_L},\quad T'_L=\frac{2n_L}{n_g+n_L}. \tag{A3}$$

n_g is the refractive index of quartz glass and n_L are the principal refractive indices of the liquid crystal when the light is polarized to L axis. These values are calculated as

$$n_Z=\frac{n_\perp n_\parallel}{\sqrt{n_\perp^2\cos^2\psi+n_\parallel^2\sin^2\psi}},\quad n_Y=n_\perp, \tag{A4}$$

where $n_\parallel$ and $n_\perp$ are the principal refractive indices of liquid crystal.

2. SmC^*_α phase

In SmC^*_α the helical pitch is smaller than wavelengths of the incident and scattered light [45]. Then the phase is optically uniaxial and the refractive index frame is identical with the layer frame. The electric field of light is given by Eqs. (A1) and (A2) as for the SmA phase.

3. SmC^* phase

SmC^* phase is optically biaxial [9] and has a helical structure. In this phase helical pitch is larger than the wavelength of the light [5,44], so that the optical elasticity axes or the refractive index frame axes are not identical with the molecular orientation frame axes. Optic elasticity axes at χ would be given by the average of the molecular orientation frame between $\chi-\pi\lambda/H$ and $\chi+\pi\lambda/H$, because the spatial resolution could be determined by the wavelength of the light λ. Hence $\hat{z}_1$ is described in the layer frame as

$$\hat{z}_1=z_1\times\begin{pmatrix}\sin\phi\langle\langle\cos\chi'\rangle\rangle\\ \sin\phi\langle\langle\sin\chi'\rangle\rangle\\ \cos\phi\end{pmatrix}, \tag{A5}$$

where $\langle\langle\cdots\rangle\rangle$ denotes statistical average from $\chi'=\chi-\pi\lambda/H$ to $\chi'=\chi+\pi\lambda/H$. $\langle\langle\cos\chi'\rangle\rangle$ and $\langle\langle\sin\chi'\rangle\rangle$ are calculated as

$$\langle\langle\cos\chi'\rangle\rangle=\int_{\chi-\pi\lambda/H}^{\chi+\pi\lambda/H}\cos\chi'\,d\chi'\Big/\int_{\chi-\pi\lambda/H}^{\chi+\pi\lambda/H}d\chi =\frac{H}{\pi\lambda}\sin\left(\frac{\pi\lambda}{H}\right)\cos\chi, \tag{A6}$$

$$\langle\langle\sin\chi'\rangle\rangle=\int_{\chi-\pi\lambda/H}^{\chi+\pi\lambda/H}\sin\chi'\,d\chi'\Big/\int_{\chi-\pi\lambda/H}^{\chi+\pi\lambda/H}d\chi =\frac{H}{\pi\lambda}\sin\left(\frac{\pi\lambda}{H}\right)\sin\chi, \tag{A7}$$

so that

$$\hat{z}_1=z_1\times\begin{pmatrix}\frac{H}{\pi\lambda}\sin\left(\frac{\pi\lambda}{H}\right)\sin\phi\cos\chi\\ \frac{H}{\pi\lambda}\sin\left(\frac{\pi\lambda}{H}\right)\sin\phi\sin\chi\\ \cos\phi\end{pmatrix}. \tag{A8}$$

In the same way as $\hat{z}_1$,

$$\hat{x}_1=x_1\times\begin{pmatrix}\frac{H}{\pi\lambda}\sin\left(\frac{\pi\lambda}{H}\right)\cos\phi\cos\chi\\ \frac{H}{\pi\lambda}\sin\left(\frac{\pi\lambda}{H}\right)\cos\phi\sin\chi\\ \cos\phi\end{pmatrix},$$

$$\hat{y}_1=y_1\times\begin{pmatrix}\frac{H}{\pi\lambda}\sin\left(\frac{\pi\lambda}{H}\right)\cos\phi\sin\chi\\ \frac{H}{\pi\lambda}\sin\left(\frac{\pi\lambda}{H}\right)\cos\phi\cos\chi\\ \cos\phi\end{pmatrix}. \tag{A9}$$

Consequently, $\mathbf{E}_{(X)}$ and $\mathbf{E}'_{(X)}$ are given by

$$\begin{aligned}\mathbf{E}_{(X)}=e^{-i\delta x_1}(&-T_Z\sin\phi\cos\psi\cos\theta\\ &+T_ZK\cos\chi\cos\phi\sin\psi\cos\theta\\ &+T_YK\sin\chi\cos\phi\sin\theta)\hat{x}_1+e^{-i\delta y_1}\\ &\times(-T_ZK\sin\chi\sin\psi\cos\theta+T_YK\cos\chi\sin\theta)\hat{y}_1\\ &+(T_Z\cos\phi\cos\psi\cos\theta+T_ZK\cos\chi\sin\phi\sin\psi\cos\theta\\ &+T_YK\sin\chi\sin\phi\sin\theta)\hat{z}_1,\end{aligned} \tag{A10}$$

$$\begin{aligned}\mathbf{E}'_{(X)}=e^{-i\delta' x_1}(&-T'_Z\sin\phi\cos\psi\cos\theta'\\ &+T'_ZK'\cos\chi\cos\phi\sin\psi\cos\theta'\\ &+T'_YK'\sin\chi\cos\phi\sin\theta')\hat{x}_1+e^{-i\delta' y_1}\\ &\times(-T'_ZK'\sin\chi\sin\psi\cos\theta'+T'_YK'\cos\chi\sin\theta')\hat{y}_1\\ &+(T'_Z\cos\phi\cos\psi\cos\theta'\end{aligned}$$

$$+T_Z'K'\cos\chi\sin\phi\sin\psi\cos\theta'$$

$$+T_Y'K'\sin\chi\sin\phi\sin\theta')\hat{z}_1, \quad \text{(A11)}$$

where

$$K=\frac{H}{\pi\lambda}\sin\left(\frac{\pi\lambda}{H}\right), \quad K'=\frac{H}{\pi\lambda'}\sin\left(\frac{\pi\lambda'}{H}\right), \quad \text{(A12)}$$

and λ and λ' are the wavelengths of the incident and the scattering light in the medium, respectively.

Though T_L and T_L' depend on χ in SmC^* phase, their variations are small enough to use Eqs. (A3) and (A4) approximately [9].

4. SmC_A^* phase

In SmC_A^* phase, ϕ is apparently zero at the spatial resolution of the light and the refractive index frame is identical with molecular orientation frame, because c is reversed in the adjacent layer. In this phase, T_L and T_L' vary as in SmC^* phase. However, the variation of $n_\perp$ is very small in this phase also [9], so that T_L and T_L' can be calculated by Eqs. (A3) and (A4) approximately. Therefore, the electric field of light is treated as in SmA phase. Hence the electric fields of the light are given by Eqs. (A1) and (A2).

5. SmC_γ^* phase

The average of the molecular tilt angle is apparently $\phi/2$ at the spatial resolution of light, because c is reversed once by the period of three layers in this phase [7–10]. This phase is optically biaxial like the SmC^* phase. Therefore the electric fields of light are obtained by substituting $\phi/2$ for ϕ in Eqs. (A10) and (A11). T_L and T_L' are approximated by Eqs. (A3) and (A4) also here.

APPENDIX B: BIAXIALITY OF ORIENTATIONAL DISTRIBUTION FUNCTION AND THE ORDER PARAMETERS

When the molecular orientational distribution function $f(\alpha,\beta,\gamma)$ has a relation of $f(\alpha,\beta,\gamma)=f(\pi+\alpha,\pi-\beta,\pi+\gamma)$, $f(\alpha,\beta,\gamma)$ can be expanded with Wigner rotation matrix in the molecular orientation frame as follows [20]:

$$f(\Omega)=\sum_{L=\text{even}}\sum_{m,m'=-L}^{L}\frac{2L+1}{8\pi^2}a_{m'm}^{(L)}D_{m'm}^{(L)}(\Omega), \quad \text{(B1)}$$

where Ω represents α, β, and γ. $a_{m'm}^{(L)}$ is given by

$$a_{m'm}^{(L)}=\int_0^{2\pi}d\alpha\int_0^{\pi}\sin\beta\,d\beta\int_0^{2\pi}d\gamma\,D_{m'm}^{(L)*}(\Omega)f(\Omega)$$

$$=\langle D_{m'm}^{(L)*}(\Omega)\rangle. \quad \text{(B2)}$$

When it is taken into account that the system has a cylindrical symmetry about Z_1 axis because of the helical structure and the Raman tensor frame is tilted against the molecular fixed frame, the polarized Raman intensities are given by the same equations (9) and (10). Here $\langle P_L(\cos\beta_{\text{app}})\rangle$ is related to $\langle D_{m'm}^{(L)*}(\Omega)\rangle$ by

$$\langle P_L(\cos\beta_{\text{app}})\rangle=\sum_{m,m'=-L}^{L}A_{m'm}^{(L)}(\phi,\alpha_0,\beta_0,\gamma_0)\langle D_{m'm}^{(L)*}(\Omega)\rangle, \quad \text{(B3)}$$

where the coefficient $A_{m'm}^{(L)}(\phi,\alpha_0,\beta_0,\gamma_0)$ is a function of ϕ, α_0, β_0, and γ_0; e.g., when $m=m'=0$, $A_{00}^{(L)}=P_L(\cos\phi)P_L(\cos\beta_0)$.

[1] A. D. L. Chandani *et al.*, Jpn. J. Appl. Phys., Part 2 **27**, L729 (1988).
[2] A. D. L. Chandani *et al.*, Jpn. J. Appl. Phys., Part 2 **28**, L1261 (1989).
[3] M. Fukui *et al.*, Jpn. J. Appl. Phys., Part 2 **28**, L849 (1989).
[4] S. Asahina *et al.*, Liq. Cryst. **23**, 339 (1997).
[5] A. D. L. Chandani *et al.*, Jpn. J. Appl. Phys., Part 2 **28**, L1265 (1989).
[6] Ch. Bahr and D. Fliegner, Phys. Rev. Lett. **70**, 1842 (1993).
[7] K. Hiraoka *et al.*, Jpn. J. Appl. Phys., Part 2 **29**, L103 (1990).
[8] J. Lee *et al.*, Jpn. J. Appl. Phys., Part 1 **29**, 1122 (1990).
[9] E. Gorecka *et al.*, Jpn. J. Appl. Phys., Part 1 **29**, 131 (1990).
[10] J. Lee *et al.*, J. Phys.: Condens. Matter **2**, SA271 (1990).
[11] P. Bak, Phys. Today **39(12)**, 38 (1986).
[12] P. Bak and J. Boehm, Phys. Rev. B **21**, 5297 (1980).
[13] T. Isozaki *et al.*, Phys. Rev. B **48**, 13 439 (1993).
[14] K. Hiraoka *et al.*, Jpn. J. Appl. Phys., Part 2 **30**, L1819 (1991).
[15] K. Hori and K. Endo, Bull. Chem. Soc. Jpn. **66**, 46 (1993).
[16] T. Nakai *et al.*, J. Phys. Chem. B **103**, 406 (1999).
[17] Y. Takanishi *et al.*, Jpn. J. Appl. Phys., Part 1 **30**, 2023 (1991).
[18] K. H. Kim, K. Ishikawa, H. Takezoe, and A. Fukuda, Phys. Rev. E **51**, 2166 (1995).
[19] K. Miyachi *et al.*, Phys. Rev. E **52**, R2153 (1995).
[20] S. Jen, N. A. Clark, P. S. Pershan, and E. B. Priestley, J. Chem. Phys. **66**, 4635 (1977).
[21] C. H. Wang, *Spectroscopy of Condensed Media* (Academic, London, 1985).
[22] *The Molecular Dynamics of Liquid Crystals*, edited by G. R. Luckhurst and C. A. Veracini (Kluwer Academic, Dordrecht, The Netherlands, 1994).
[23] M. Constant and D. Decoster, J. Chem. Phys. **76**, 1708 (1982).
[24] K. H. Kim *et al.*, Jpn. J. Appl. Phys., Part 1 **33**, 5850 (1994).
[25] R. Seeliger, H. Haspeklo, and F. Noack, Mol. Phys. **49**, 1039 (1983).
[26] K. Miyano, J. Chem. Phys. **69**, 4807 (1978).
[27] S. N. Prasad and S. Venugopalan, J. Chem. Phys. **75**, 3033 (1981).
[28] G. R. Luckhurst and R. N. Yeates, J. Chem. Soc., Faraday Trans. 2 **72**, 996 (1976).
[29] S. Miyajima and T. Hosokawa, Phys. Rev. B **52**, 4060 (1995).

[30] T. Nakai, H. Fujimori, D. Kuwahara, and S. Miyajima, J. Phys. Chem. B **103**, 417 (1999).
[31] M. P. Fontana, B. Rosi, N. Kirov, and I. Dozov, Phys. Rev. A **33**, 4132 (1986).
[32] B. Park *et al.*, Jpn. J. Appl. Phys., Part 1 **38**, 1474 (1999).
[33] A. Suzuki *et al.*, Jpn. J. Appl. Phys., Part 2 **29**, L336 (1990).
[34] Y. Ouchi *et al.*, Jpn. J. Appl. Phys., Part 2 **27**, L725 (1988).
[35] T. P. Rieker *et al.*, Phys. Rev. Lett. **59**, 2658 (1987).
[36] Y. Takanishi, Y. Ouchi, H. Takezoe, and A. Fukuda, Jpn. J. Appl. Phys., Part 2 **28**, L487 (1989).
[37] Y. Ouchi, Y. Takanishi, H. Takezoe, and A. Fukuda, Jpn. J. Appl. Phys., Part 1 **28**, 2547 (1989).
[38] M. Johno *et al.*, Jpn. J. Appl. Phys., Part 2 **29**, L111 (1990).
[39] K. Hiraoka *et al.*, Jpn. J. Appl. Phys., Part 2 **29**, L1473 (1990).
[40] M. J. Frisch *et al.*, GAUSSIAN 94, Development version (Gaussian, Inc., Pittsburgh, PA, 1994).
[41] E. Sackmann *et al.*, J. Am. Chem. Soc. **90**, 3567 (1968).
[42] K. Kondo *et al.*, Jpn. J. Appl. Phys., Part 1 **21**, 224 (1982).
[43] K. H. Kim *et al.*, Liq. Cryst. **16**, 185 (1994).
[44] J. Li, H. Takezoe, and A. Fukuda, Jpn. J. Appl. Phys., Part 1 **30**, 532 (1991).
[45] V. Laux *et al.*, Ferroelectrics **179**, 25 (1996).